

Clustering of Galaxies at High Redshifts

J.S.Bagla

Institute of Astronomy, University of Cambridge, Madingley Road, Cambridge CB3 0HA, U.K.

E-mail: jasjeet@ast.cam.ac.uk

1 February 2008

ABSTRACT

Recent observations show a large concentration of galaxies at high redshift. At first sight strong clustering of galaxies at high redshifts seems to be in contradiction with the models of structure formation. In this paper we show that such structures are a manifestation of the strong clustering of rare peaks in the density field. We compute the frequency of occurrence of such large concentrations of galaxies in some models of structure formation.

Key words: Galaxies : Formation – Cosmology : Theory – Early Universe, Large Scale Structure of the Universe

1 INTRODUCTION

Observations of galaxies at high redshifts, around $z = 3$, in a contiguous region of sky (Steidel et al 1997) show a marked concentration in a region of width $\Delta z = 0.04$, or $\Delta v = 3000 \text{ km s}^{-1}$. The angular size of the region probed is $9' \times 18'$ and within this region the galaxies contributing to the peak are distributed randomly in about half the area. A quasar is also present in this wall like structure. The clustering in redshift space is estimated to have a confidence level of 99.8%. Steidel et al. (1997) point out that clustering at such large scales, in most models of galaxy formation, requires high bias to explain the observed structure.

First galaxies to form in the universe correspond to the deepest potential wells or the highest peaks in the initial density distribution. It is well known that these rare peaks cluster more strongly than, say, the typical peaks (Bardeen et. al. 1986). Therefore, at early times, when only rare peaks have collapsed into structures like galaxies, we expect these objects to show significant clustering. The epoch when typical halos of a given mass scale M collapse is characterised by $\sigma(M, z) \simeq \delta_c$ (Press and Schechter 1975). It is customary to use $\delta_c = 1.69$ as a spherical perturbation virialises when the linearly extrapolated density contrast equals δ_c (Gunn and Gott 1972). If we define a quantity $\nu(M, z) = \delta_c / \sigma(M, z)$, then we can say that typical halos of mass M collapse when $\nu(M) \simeq 1$. For $\nu \gg 1$, only the rare peaks of the given mass scale have collapsed and these tend to cluster very strongly. In this paper, we study clustering of halos at $z \approx 3$ and compare it with the constraint set by the observation of Steidel et al. (1997) for some models of structure formation.

We assume, that the galaxy distribution and the halo distribution are identical. This may not be true, especially at small scales where astrophysical processes play an important role. However, including these processes requires more

detailed modelling which, in turn, requires more assumptions. Therefore, we will restrict the present study to the study of halo distribution at high redshifts.

We address the following questions here:

- Is the clustering of dark matters halos in models of structure formation sufficiently strong to explain the observed concentration of galaxies?
- What is the frequency with which we may expect to see a 3σ excess for the number of halos if we simulate the observations of galaxies using numerical simulations?

2 CLUSTERING OF HALOS

We can study the clustering of halos using numerical simulations. For this particular study we choose the Λ CDM model with the shape parameter $\Gamma = 0.5$ (Efstathiou, Bond and White 1992). We normalise the power spectrum so that $\sigma_8 = \sigma(8h^{-1} \text{Mpc}, z = 0) = 0.6$. Most models have more power at the relevant scales as compared to this, and if this model provide enough clustering at $z = 3$, most other models can do that too.

The observed number density of Lyman break galaxies is $2.9 \times 10^{-3} h^3 \text{Mpc}^{-3}$ in the Einstein-de Sitter Universe. This implies a halo mass of about $5 \times 10^{12} M_\odot$ for the Λ CDM model (Press and Schechter 1975). Using this mass for halos is same as assuming that all halos host Lyman break galaxies. In order to relax this assumption, we choose a lower halo mass, $M_{\text{halo}} \geq 7 \times 10^{11} M_\odot$. Thus less than one in ten of these halos host Lyman break galaxies. In absence of any alternative, we assume that galaxies are distributed randomly amongst these halos and hence have the same clustering properties.

We quantify the clustering of halos with the averaged two point correlation function. This is defined as

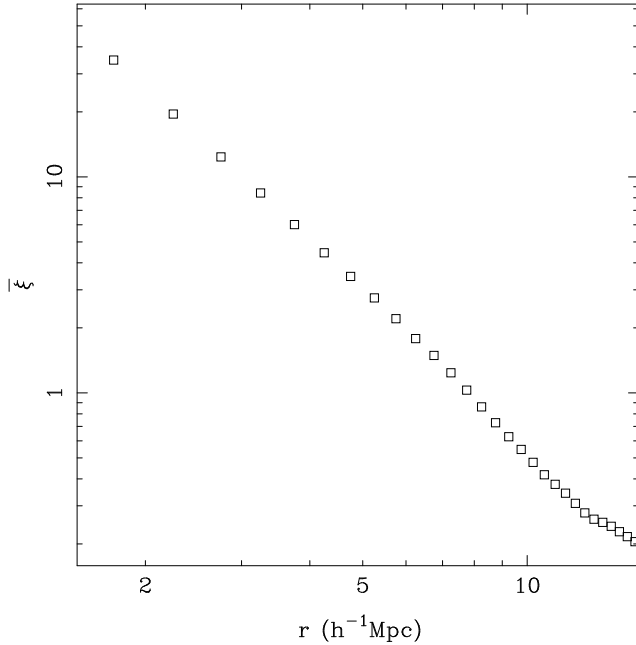


Figure 1. This figure shows the averaged two point correlation function for halos of mass $M_{halo} \geq 7 \times 10^{11} M_{\odot}$ at $z = 3$. The x-axis shows the comoving scale in units of $h^{-1} \text{Mpc}$. The amplitude of the halo correlation function is comparable to the galaxy correlation function at $z = 0$, i.e. it is much higher than the amplitude of mass correlation function at $z = 3$.

$$\bar{\xi}(r) = \frac{3}{r^3} \int_0^r x^2 \xi(x) dx = \frac{3J_3(r)}{r^3} \quad (1)$$

where $\xi(x)$ is the two point correlation function.

Halos are identified using the Friends-of-Friends (FOF) algorithm with a linking length of 0.2 (over-density of 60). Fig.1 shows the averaged correlation function as a function of scale for these halos at redshift $z = 3$. If the number density of these halos is \bar{n} , then the number of halos within distance r from a typical halo is $4\pi r^3 \bar{n} (1 + \bar{\xi}(r))/3$. Thus we expect to see twice the average number in a sphere of radius $8h^{-1} \text{Mpc}$ around a typical halo. Some halos will have more neighbours than a typical halo. Therefore, an excess of a factor four in one bin is not very surprising.

The large amplitude of correlation function is not completely surprising. Analytical models for evolution of bias for halos also predict that bias increases with increasing redshift (For example, see Matarrese et al. 1997). These predictions suggest that the amplitude of halo correlation function decreases very slowly with increasing redshift. However, most of these models do not predict the halo correlation function at $z = 3$ to be as strong as the present day galaxy correlation function (Bagla 1997).

3 SYNTHETIC OBSERVATIONS

In this section, we will simulate observations using N-Body simulations. We will restrict our study to the CDM class of models. In particular, we will study clustering in the standard CDM model ($\Gamma = 0.5$) and a variant of SCDM that reproduces the observed correlation function out to

large scales ($\Gamma = 0.3$). These models are normalised so that $\sigma_8 = \sigma(8h^{-1} \text{Mpc}, z = 0) = 0.6$. To describe differences induced by a higher normalisation we will use the same models with $\sigma_8 = 1$. The background cosmology is assumed to be $\Omega = 1$, $H_0 = 50 \text{km Mpc}^{-1} \text{s}^{-1}$. We will specify all scales in the comoving coordinates.

The observations indicate a very large scale for the concentration of galaxies. In the Einstein deSitter model $\Delta z = 0.04$ translates to $15h^{-1} \text{Mpc}$. The observed angular extent of the structure in question is greater than or equal to $8' \times 11'$. (One arc minute corresponds to $0.87h^{-1} \text{Mpc}$ at $z = 3$.) To study clustering on such large scales we need to simulate a very large volume and we chose to work with a simulation box of size $166h^{-1} \text{Mpc}$. All simulations were done using 128^3 particles so that mass of each N-Body particle was approximately $10^{12} M_{\odot}$. All N-Body simulations used here were done using a Particle-Mesh code.

To simulate “observations” of high redshift galaxies we use the following method.

- As galaxies form in regions with high density, we begin by isolating such regions in the simulation volume.
- We project the particles in the selected regions in redshift space by assuming that one of the axes is aligned along the line of sight. Velocity along the line of sight and the Hubble redshift combine to give the total effective redshift of each particle.

$$1 + z_{tot} = (1 + z_{hub}) (1 + z_{pec}) \quad (2)$$

Here $z_{pec} = v_p/c$ with c the speed of light and v_p the component of the peculiar velocity of the particle along the line of sight.

- We then view the selected particles around a large number of lines of sight. For each line of sight all particles within a square region of $10' \times 10'$ are included in the field of view. The redshift distribution of these particles is then analysed for a large number of fields of view.

- We smooth the distribution in redshift by using a top hat window of width $\Delta z = 0.04$. We search for peaks in the smoothed distribution. As the correspondence between particles and galaxies is not very clear, we will measure peaks from the average amplitude in units of the standard deviation σ .

We are interested in clustering at large scales and therefore we have to use a large simulation volume. This implies that the mass of individual particles in the simulation is considerably larger than the mass associated with the galaxies we are studying. This clearly makes it difficult to identify galaxies directly and we can only try to isolate regions where such galaxies could have formed. Therefore, we work with three density thresholds: (1) $\bar{\varrho}_c = 0$, i.e. no cutoff; (2) $\bar{\varrho}_c = 2\varrho_b$, i.e. we will select regions with $\delta \geq 1$. Here ϱ_b is the background density and δ is the density contrast. And, (3) $\bar{\varrho}_c = 4\varrho_b$, or $\delta \geq 3$. As we are using very low thresholds, the frequency of occurrence of large concentrations of galaxies computed here is essentially a lower limit.

Our aim here is to search for clustering at large scales in redshift and the width of the structure we hope to reproduce is $\Delta z = 0.04$. However, it is useful to start with smaller bins and average over the neighbouring bins with a top hat filter. This ensures that all high peaks are picked out.

We group the particles in each field of view in bins of

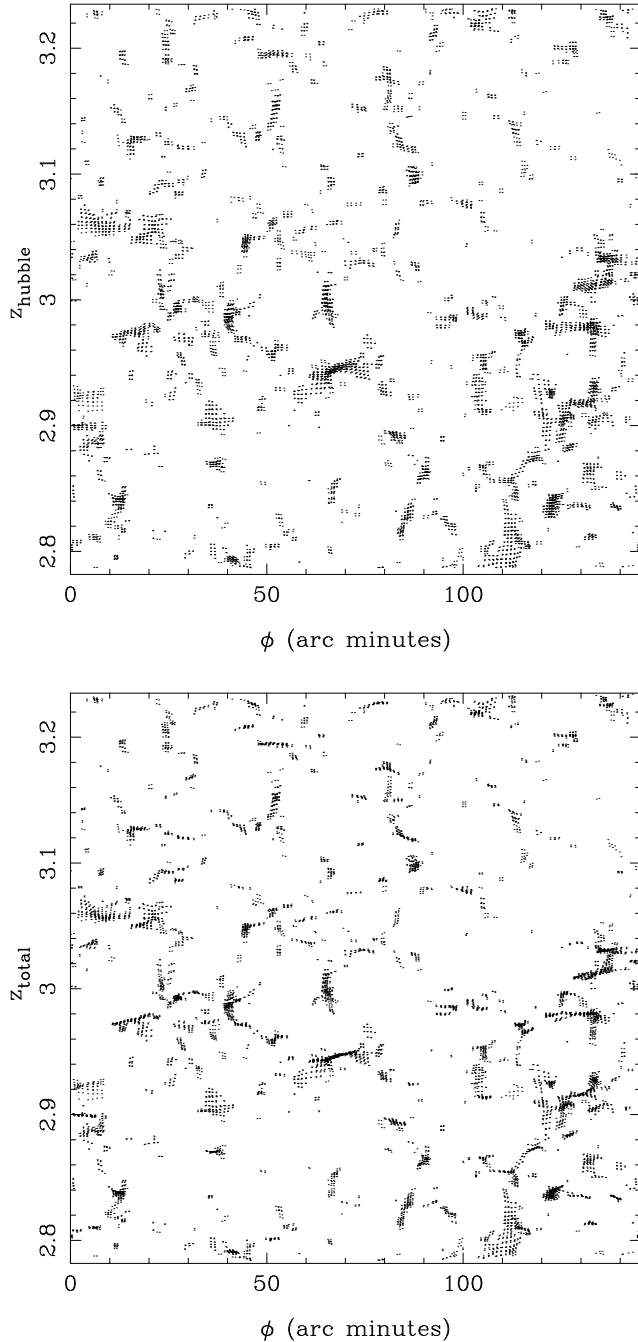


Figure 2. This figure shows the dense structures selected using a threshold $\bar{\rho}_c = 4\rho_b$ in real as well as redshift space. The model used in these simulations is CDM with $\Gamma = 0.5$, normalised to $\sigma_8 = 0.6$. The figures show projected distribution of a slice of thickness $10'$. The top panel shows the particles in real space and for comparison with the second panel and observations, we have used the cosmological redshift and angle ϕ as coordinates. The lower panel shows the same set of particles in redshift space. Here $1 + z_{tot} = (1 + z_{hub})(1 + z_{pec})$, where $z_{pec} = v_p/c$ with c as the speed of light and v_p the component of peculiar velocity along the line of sight. It is obvious from this figure that redshift space distortions operate on much smaller scales than $\Delta z = 0.04$. It is also clear that there are clearly some structures with an angular extent greater than $10'$, size of the observed concentration.

500 km s^{-1} . We then combined six bins around each of the smaller bins to get a distribution with $\Delta z = 0.04$ sampled at every 500 km s^{-1} . We scan this distribution for locating maxima and in order to avoid over-counting high peaks, we ensure that a given bin has the largest number of particles as compared to bins within $\Delta z = 0.02$ on either side. The amplitude of peaks is measured from the average in units of standard deviation – the average and standard deviation are obtained from a large number of “fields of view” through the given simulation box.

4 RESULTS

We have plotted a slice from an N-Body simulation in fig.2. This figure shows the projection of a slice from a CDM simulation with $\Gamma = 0.5$ and $\sigma_8 = 0.6$. The particles shown here are located in regions with $\delta \geq 3$. The projection is shown in both real and redshift space. For easy comparison with the relevant observations, we have used angular size and redshift as the coordinates. The thickness of this slice is $10'$. The top panel shows the distribution of particles in real space and the lower panel shows the same set of particles in redshift space. It is clear that redshift space distortion tends to squeeze many structures into a thin sheet perpendicular to the line of sight. However, the scale where this effect is important is much smaller than $\Delta z = 0.04$. The sizes of largest structures – angular sizes as well as the extent in redshift – and the effects of redshift space distortion can be seen clearly. Redshift space distortions play a very important role at small scales (McGill 1990a, 1990b) but for the scales that we are interested in, i.e. $\Delta z = 0.04$, these effects are smoothed out. At these scales, the frequency with which such structures appear is identical in the real and redshift space.

Fig.3 shows the redshift distribution in two fields of view obtained using the method outlined in §3. These particular examples were chosen to exhibit the variety of distributions and peaks seen in such systems. In one case we see a semi-periodic set of peaks whereas in the other case we see only one isolated peak.

Table 1 lists the frequency of occurrence of $N\sigma$ peaks above average in the redshift space distribution. Here we have extrapolated from the range of redshift covered by the simulation to that used in Steidel et al. (1997) to facilitate comparison. We can summarise the conclusions as follows:

- Models with same normalisation predict similar frequency of occurrence for peaks with $N\sigma$ more particles than average. This is to be expected as both models have similar power at the relevant scale.
- Models with higher normalisation predict a higher frequency of occurrence for the unbiased case.
- Models with higher normalisation predict a lower frequency of occurrence for 5σ peaks above average for the high density threshold. This can be understood if the statistical bias depends only on ν defined in the introduction. This is small for models with the higher normalisation, and hence we do not see the effect of strong clustering of rare peaks.

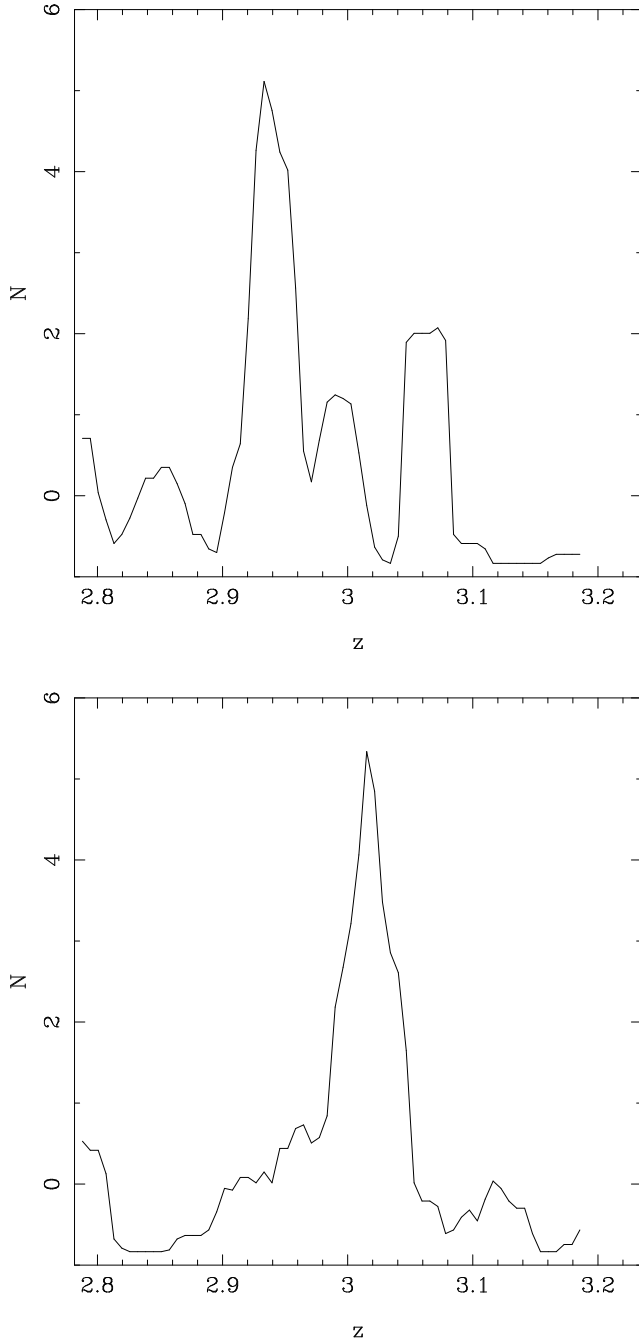


Figure 3. Distribution of objects in redshift space. These panels show the redshift distribution in two $10' \times 10'$ fields of view through a simulation volume. These are from the simulation used in fig.2. These frames show a few high peaks in the distribution. The y axis is the height of a peak measured from the average in units of standard deviation σ . The curve shows an average over $\Delta z = 0.04$ sampled at intervals of $\Delta z = 0.0067$.

5 DISCUSSION

We have shown that the observations of strong clustering of galaxies at high redshifts are not in conflict with the popular models of structure formation. We have demonstrated this in two different ways: first by showing that the bias can indeed be very large at early times. We have also generated synthetic observations in a few models and have shown

Γ	σ_8	δ_c	$N = 3$	$N = 4$	$N = 5$
0.5	0.6	—	0.45	0.07	0.01
0.5	0.6	1	0.64	0.11	0.01
0.5	0.6	3	1.01	0.45	0.18
0.3	0.6	—	0.46	0.07	0.01
0.3	0.6	1	0.77	0.19	0.04
0.3	0.6	3	0.87	0.51	0.24
0.5	1.0	—	0.71	0.16	0.03
0.5	1.0	1	0.72	0.18	0.04
0.5	1.0	3	0.99	0.34	0.12
0.3	1.0	—	0.73	0.16	0.03
0.3	1.0	1	0.73	0.17	0.04
0.3	1.0	3	1.00	0.34	0.12

Table 1. This table lists the frequency of $N\sigma$ peaks above average in the models of structure formation studied here. The first two columns refer to the parameters of the model, the shape parameter Γ and normalisation σ_8 . The third column lists the threshold in density contrast used to select particles. The last three columns list the frequency for finding 3, 4 and 5 σ peaks above average in fields of view of $10' \times 10'$ and redshift range $2 \leq z \leq 3.5$.

that the frequency of occurrence of large concentrations of galaxies is compatible with observations.

Fig.2 suggests that still larger structures maybe found in future searches. The distribution of sizes of largest structures in surveys at high redshift – both angular size and the extent in redshift – may be used to discriminate between different models.

Strong clustering of galaxies at high redshifts implies that the galaxy clustering evolves in a very different manner as compared to clustering in the underlying mass distribution. A detailed study of the evolution of halo clustering and its implications for galaxy clustering has been presented elsewhere (Bagla 1997).

ACKNOWLEDGEMENT

I thank Max Pettini for drawing my attention to this observation. I acknowledge the support of PPARC fellowship at the Institute of Astronomy.

REFERENCES

- Bagla J.S. 1997, astro-ph/9711081, Submitted to MNRAS
- Bardeen J.M., Bond J.R., Kaiser N. and Szalay A.S. 1986, ApJ 304, 15
- Efstathiou G., Bond J.R. and White S.D.M. 1992, MNRAS 258, 1p
- Gunn J.E. and Gott J.R. 1972, ApJ 176, 1
- Matarrese S., Coles P., Lucchin F. and Moscardini L. 1997, MNRAS 286, 115
- McGill C. 1990a, MNRAS 242, 428
- McGill C. 1990b, MNRAS 242, 544
- Press W.H. and Schechter P. 1975, ApJ 187, 452
- Steidel C.C., Adelberger K.L., Dickinson M., Giavalisco M., Pettini M. and Kellogg M. 1997, Submitted to ApJ.